Modulated Rashba-Dresselhaus Spin-Orbit Coupling for Topology Control and Analog Simulations

Pavel Kokhanchik,[1,*] Dmitry Solnyshkov,[1,2] Thilo Stöferle,[3] Barbara Piętka,[4] Jacek Szczytko,[4] and Guillaume Malpuech[1]

[1]*Institut Pascal, Université Clermont Auvergne, CNRS, Clermont INP, F-63000 Clermont-Ferrand, France*
[2]*Institut Universitaire de France (IUF), 75231 Paris, France*
[3]*IBM Research Europe–Zurich, CH-8803 Rüschlikon, Switzerland*
[4]*Institute of Experimental Physics, Faculty of Physics, University of Warsaw, Pasteura 5, 02-093 Warsaw, Poland*

(Received 2 June 2022; accepted 28 October 2022; published 5 December 2022)

We show theoretically that Rashba-Dresselhaus spin-orbit coupling (RDSOC) in lattices acts as a synthetic gauge field. This allows us to control both the phase and the magnitude of tunneling coefficients between sites, which is the key ingredient to implement topological Hamitonians and spin lattices useful for simulation perpectives. We use liquid crystal based microcavities in which RDSOC can be switched on and off as a model platform. We propose a realistic scheme for implementation of a Su-Schrieffer-Heeger chain in which the edge states existence can be tuned, and a Harper-Hofstadter model with a tunable contrasted flux for each (pseudo)spin component. We further show that a transverse-field Ising model and classical XY Hamiltonian with tunable parameters can be implemented, opening up prospects for analog physics, simulations, and optimization.

DOI: 10.1103/PhysRevLett.129.246801

Artificial gauge fields have been synthesized in various platforms for more than a decade [1]. They constitute the basis of synthetic topological matter [2] and quantum simulations [3]. Artificial gauge fields allow one to control complex hopping amplitudes between lattice sites, enabling the implementation of topological Hamiltonians, such as Harper-Hofstadter [4–8] or Haldane [9] models. On the other hand, classical and quantum simulations are often based on mapping tight-binding Hamiltonians to spin models, such as Ising [10] or XY models [11], where the spin orientation is represented by the phase of the wave function [12]. The ground state and dynamics of these spin models can be linked with a huge variety of computational problems [13], but this requires a versatile control of the magnitude of the couplings in a graph [14], either between spins in an original spin model or between lattice sites in a mapped tight-binding model. The key ingredient for implementing artificial gauge fields and controlling the phases and magnitudes of these coupling coefficients is the spin-orbit coupling (SOC).

In photonics, the vectorial nature of light modes with transverse-electric (TE) and transverse-magnetic (TM) polarizations is responsible for the existence of an intrinsic SOC [15–22]. The combination of photonic SOC with broken time-reversal symmetry (TRS) achieved through the Faraday effect (effective Zeeman splitting) makes 2D cavity modes [23] topologically nontrivial [24–28], characterized by Chern numbers ± 2. Topological gaps and related unidirectional edge modes appear when these bulk topological modes are placed in an appropriate photonic lattice [29–35]. The described effect simulates the quantum anomalous Hall effect [9], being the foundation of topological photonics. The field is then considerably enriched with the proposals and realizations of the quantum pseudospin Hall effect which does not require TRS breaking. In such cases, the pseudospin involved can be the angular momentum of the ring resonator [6,7], polarization [36,37], and sublattice (e.g., valley) pseudospins, both in 2D [38–40] and 1D, essentially in that case through the use of dimer chains described by a Su-Schrieffer-Heeger (SSH) Hamiltonian [41–45]. The SSH Hamiltonian is the simplest topological model supporting topological edge modes. Contrary to 2D topological models, such as the Harper-Hofstadter model, it is based on tunneling amplitude modulation instead of phase modulation.

A new type of photonic SOC being a superposition of Rashba [46] and Dresselhaus [47] SOCs (RDSOC) with equal strength has been recently demonstrated. It was initially studied in solid-state physics [48,49], and realized with cold atoms [50]. In photonics, it was implemented first in 1D settings such as metasurfaces with broken inversion symmetry [51–54], chiral photonic crystals [55], photonic lattices of waveguide arrays [56], and asymmetric polariton waveguides [57]. Most recently, its realization has been reported in planar microcavities either filled with liquid crystals (LCs) [58] or with a birefringent organic crystal [59] where it was called emergent optical activity. Together with TE-TM SOC, effective Zeeman field, and in-plane potential (lattices), RDSOC plays the role of a

supplementary control knob for implementing effective Hamiltonians of interest and for controlling the mode topology [60]. The crucial property offered by LC microcavities [61–65] is the tunability of the modes by means of the external voltage applied to the LC molecules. This allows one to switch the RDSOC on and off electrically. So far, the effect of the RDSOC (which in 1D is equivalent to the Rashba SOC) in the SSH setting has been theoretically discussed in the context of electronic systems [61–65], but only for a homogeneous or small Rashba SOC resulting in no topological effects.

In this Letter, we theoretically study tight-binding Hamiltonians for massive (pseudo)spinor particles including RDSOC and in-plane (effective) magnetic field. Depending on the value of the latter, we show that RDSOC controls either the phase or the amplitude of the tunneling coefficients between sites. We show that a photonic implementation based on LC cavities is suitable to control both the on-site in-plane field and the RDSOC magnitude in the links by the applied voltage. For a 1D dimer chain (SSH), the tuning of the tunneling amplitude allows us to switch between a trivial phase and a topological phase hosting edge modes. The access to negative tunnelings allows us to emulate the transverse-field Ising model (TFIM) in a whole parameter space. The practical feasibility of this 1D setting is further supported by full 2D continuous simulations using realistic experimental parameters. In 2D lattices, the control of the phases of individual tunnelings allows emulation of the TRS-preserving Harper-Hofstadter Hamiltonian with tunable flux per plaquette having opposite signs for different spin components. The control of tunneling amplitude allows a mapping to the classical XY Hamiltonian possessing a broad range of simulation perspectives.

A generic Hamiltonian describing 2D massive particles with 2 internal (pseudo)spin components including RDSOC reads as follows:

$$\hat{H}_0(\mathbf{k}) = \frac{\hbar^2\mathbf{k}^2}{2m} - 2\alpha k_x\hat{\sigma}_z + \delta\hat{\sigma}_x, \tag{1}$$

where m is the mass, $\mathbf{k} = (k_x, k_y)$, k_x and k_y are the wave vector components, $\hat{\sigma}_x$ ($\hat{\sigma}_z$) is the first (third) Pauli matrix, $-2\alpha k_x\hat{\sigma}_z$ is the RDSOC with magnitude α, and δ is the splitting between $\hat{\sigma}_x$ components of particle (pseudo)spin. This Hamiltonian describes electrons [48,49], cold atoms [50], and photons in planar microcavities with large linear birefringence [58,59]. In photonic microcavities, birefringence provides a large-scale splitting bringing in resonance two modes of different parity (typically $N+1$ and N, where N is the quantization number of the longitudinal Fabry-Perot mode) which creates RDSOC. $\delta = (E_{Y,N+1} - E_{X,N})/2$ is a small-scale remaining polarization splitting.

The RDSOC acts as an effective Zeeman splitting proportional to one projection of the wave vector (here k_x), like optical activity [59]. Figures 1(b) and 1(c) show the cross section $k_y = 0$ of the energy bands for $\delta = 0$ and $\delta \neq 0$, respectively. Along the k_y axis the splitting is absent and the modes are degenerate [Fig. 1(a)].

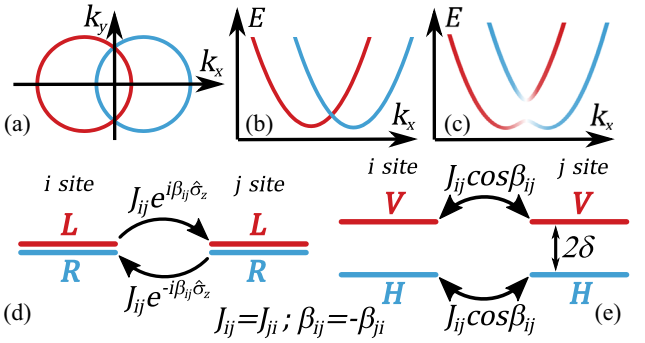

FIG. 1. Two eigenmodes of $\hat{H}_0(k)$ at a given energy (a) and along k_x for $\delta = 0$ (b) and $\delta \neq 0$ (c) (color shows circular polarization degree); regimes of tunneling phase ($\delta = 0$) (d) and amplitude (large δ) (e) control.

We next consider a tight-binding description of the coupling between two sites i and j, each hosting (pseudo)spin $1/2$ particles. If the link has an angle θ with respect to the RDSOC direction, the two eigenmodes of $\hat{\sigma}_z$ acquire opposite Aharonov-Casher phase $\pm\beta_{ij}(\theta)$ while propagating along the link [64,66]:

$$\beta_{ij}(\theta) = \frac{\alpha a}{\hbar^2/2m}\cos\theta, \tag{2}$$

with the link length a. The tunneling coefficient reads $J_{ij}e^{i\beta_{ij}\hat{\sigma}_z}$ [Fig. 1(d)], which can be understood as the action of a spin-dependent synthetic gauge potential. Importantly, in the limit of large δ [Fig. 1(e)], the two eigenstates of a site are well separated (eigenstates of $\hat{\sigma}_x$). In that case, each site can be treated as hosting a scalar particle (single spin projection) and the tunneling amplitude reduces to $J_{ij}\cos\beta_{ij}$. It shows that a modulation of RDSOC amplitude α or orientation θ allows us to tune the magnitude and sign of the tunneling coefficient.

We now consider the Hamiltonian of an arbitrary lattice which reads

$$\hat{H}_{\text{lattice}} = \sum_{i\neq j} J_{ij}e^{i\beta_{ij}\hat{\sigma}_z}|j\rangle\langle i| + \delta\hat{\sigma}_x|i\rangle\langle i|. \tag{3}$$

In the large δ limit, it is possible to project the Hamiltonian on an eigenstate of $\hat{\sigma}_x$ as

$$\hat{H}^{\text{reduced}}_{\text{lattice}} = \sum_{i\neq j} J_{ij}\cos\beta_{ij}|j\rangle\langle i|. \tag{4}$$

We now study a specific simple example of RDSOC modulation, showing that it allows us to control the topological properties of a 1D system. The system

proposed is a zigzag chain with a period d, shown in Fig. 2(a). The direction of RDSOC is constant in space (red arrow). Tunnelings (intracell J_1 and intercell J_2) as well as angles which they form with RDSOC direction (θ_1 and θ_2) are staggered. These angles control the phases β_1 and β_2. The unit cell consists of two lattice sites A and B. The RDSOC couples the sublattice pseudospin (A and B) and particle (pseudo)spin ($+$ and $-$). The spinor chain is more complex than a spinless SSH chain. The Hamiltonian (3) reduces to a 4×4 Hamiltonian which in the basis $(A_+, A_-, B_+, B_-)^T$ reads

$$\hat{H}_{\sigma\mathrm{SSH}}(k_x) = -\begin{pmatrix} 0 & \delta & J_1 e^{i\beta_1} + J_2 e^{-i\beta_2} e^{-ik_x d} & 0 \\ \delta & 0 & 0 & J_1 e^{-i\beta_1} + J_2 e^{i\beta_2} e^{-ik_x d} \\ J_1 e^{-i\beta_1} + J_2 e^{i\beta_2} e^{ik_x d} & 0 & 0 & \delta \\ 0 & J_1 e^{i\beta_1} + J_2 e^{-i\beta_2} e^{ik_x d} & \delta & 0 \end{pmatrix}. \quad (5)$$

The eigenvalues are

$$E(k_x) = \pm\Big[\delta^2 + \rho_1^2 + \rho_2^2 \pm 2\rho_1\sqrt{\delta^2 + \rho_2^2 \sin^2(\varphi_2 - \varphi_1)}\Big]^{1/2}, \quad (6)$$

where $\rho_1 e^{i\varphi_1} = J_1\cos\beta_1 + J_2\cos\beta_2\, e^{-ik_x d}$ and $\rho_2 e^{i\varphi_2} = J_1\sin\beta_1 - J_2\sin\beta_2\, e^{-ik_x d}$ describe the copolarized and cross-polarized tunnelings in the linear polarization basis [67]. The RDSOC allows us to modulate the intracell, intercell copolarized and cross-polarized tunnelings via $\cos\beta_i$ and $\sin\beta_i$. The four bands are separated in two pairs, symmetric with respect to $E = 0$ because of the global chiral symmetry of the model. If $\delta \gg J_1, J_2$, it is possible to use the projected Hamiltonian (4). In that case each doublet is linearly polarized and becomes described by a standard SSH Hamiltonian which for the lower H-polarized doublet reads [67]

$$\hat{H}_{\mathrm{SSH}}(k_x) \approx -\begin{pmatrix} \delta & J_1\cos\beta_1 + J_2\cos\beta_2 e^{-ik_x d} \\ \text{c.c.} & \delta \end{pmatrix}, \quad (7)$$

where c.c. stands for complex conjugate. Thus, modulated RDSOC reduces the intracell (intercell) tunneling by a factor $\cos\beta_1 (\cos\beta_2)$. It allows us to transform a monomer chain ($J_1 = J_2$) into a dimer chain or to swap relations between the links changing the chain topology, characterized by a topological invariant called the Zak phase [67,68]. The Zak phase value (0 or π) determines the absence or presence of edge states. In spinless SSH, edge states exist if $J_1 - J_2 < 0$ (chain ending with a weak link). With RDSOC, the topology is nontrivial when

$$|J_1\cos\beta_1| - |J_2\cos\beta_2| < 0. \quad (8)$$

This condition is valid in the general case [Eq. (5)] and not only for high δ. The topological transition occurs when $J_1\cos\beta_1 = \pm J_2\cos\beta_2$, which corresponds to the closing of the lowest gap [$\rho_1 = 0$ in Eq. (6)]. $J_1\cos\beta_1 = J_2\cos\beta_2$ corresponds to a gap closing at the edges of the Brillouin zone ($k_x = \pm\pi/d$, analogously to spinless SSH), whereas $J_1\cos\beta_1 = -J_2\cos\beta_2$ corresponds to a gap closing at $k_x = 0$. If a spinless SSH chain is topologically trivial, the same chain with modulated RDSOC could be either nontrivial or trivial, depending on the values of β_1 and β_2.

Figure 2(b) shows the energy bands computed in the large δ limit for $J_1 = 2$, $J_2 = 1$, $\beta_2 = 0$, and for different values of β_1 (from now on called β). The critical β values

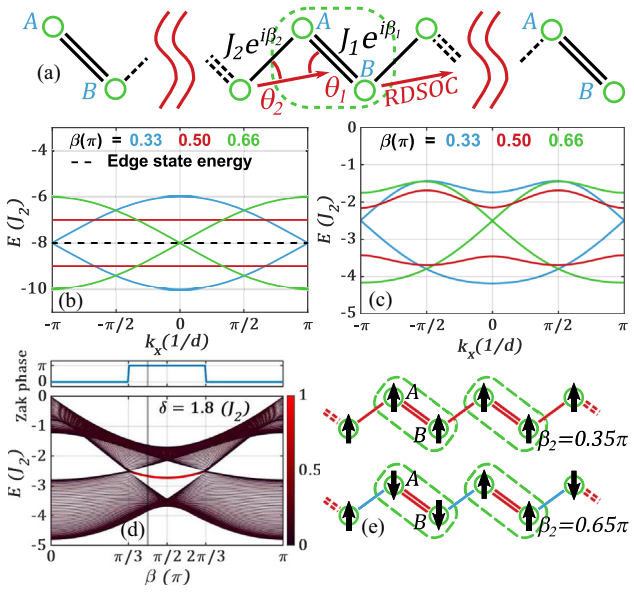

FIG. 2. (a) The scheme of SSH chain with RDSOC; the dispersion of reduced Hamiltonian (b) [Eq. (7), $\delta = 8$] and general SSH Hamiltonian (c) [Eq. (5), $\delta = 1.8$] with staggered RDSOC for several values of β (for all β, see Ref. [67]); (d) energy spectrum of finite SSH chain and Zak phase of the corresponding bulk dispersion lowest band depending on phase β produced by RDSOC (the color scale shows the edge localization); (e) SSH chain corresponding to ferromagnetic (top) and antiferromagnetic (bottom) phases of TFIM: black arrows correspond to ground state wave function phase; red (blue) shows positive (negative) couplings.

for which the band topology is changing are $\pi/3$ and $2\pi/3$, which corresponds to a gap closing at $k_x = \pm\pi/d$ and $k_x = 0$, respectively. In between these β values, a topological band gap is opened. The edge states lie in the middle of this gap because the reduced 2×2 Hamiltonian (7) preserves the chiral symmetry. Precisely at $\beta = \pi/2$, the interference induced by the RDSOC completely suppresses copolarized tunneling through the "strong" link. The corresponding band gap reaches its maximum value $2J_2$ and the bands are completely flat. Figure 2(c) shows the finite δ case, where all four bands have to be taken into account [same parameters as for Fig. 2(b)]. For any δ, the gap is again closing at $k_x = \pm\pi/d$ for $\beta = \pi/3$ and at $k_x = 0$ for $\beta = 2\pi/3$. The maximal gap value is still at $\beta = \pi/2$, but it is smaller than $2J_2$. There is no symmetry within the doublet and the edge states are not at the center of the gap. All these features are summarized in Fig. 2(d) showing the energy spectrum versus β and the corresponding Zak phase of a finite chain. A trivial gap (zero Zak phase) is present from $\beta = 0$ to $\beta = \pi/3$ where the gap closes, then immediately reopens as a topological gap persisting for $\beta \in [\pi/3; 2\pi/3]$ (the edge state energy is shown in red). The gap closes at $\beta = 2\pi/3$, becoming topologically trivial again. For $\delta < |J_1 \cos\beta|$, the bands are overlapping (not crossing). There is no real gap anymore, and therefore no protected edge states. In the case of nontrivial topology the edge states exhibit period doubling due to the particular dispersion shape [67].

Another interesting possibility offered by the tuning of tunnelings is the implementation of the mapping between the Hamiltonian (7) and the TFIM—the fundamental quantum many-body model describing the transition between ordered (ferromagnetic or antiferromagnetic) and disordered (paramagnetic) phases [69–73]. The TFIM Hamiltonian reads

$$\hat{H}_{\mathrm{TFIM}} = -J' \sum_i \hat{\sigma}_i^z \hat{\sigma}_{i+1}^z - h \sum_i \hat{\sigma}_i^x, \tag{9}$$

where J' is the coupling term, h is a transverse magnetic field, and i is the site index. After applying the Jordan-Wigner transformation, the mapping between Hamiltonians (7) and (9) is $J' = J_2 \cos\beta_2, h = J_1 \cos\beta_1$. As shown in Fig. 2(e), where the spin orientation on each site is given by the phase of the wave function, the sign modulation of tunnelings provided by RDSOC allows us to achieve both ferromagnetic and antiferromagnetic configurations, which is not the case in TFIM based on usual SSH. Thus, tunneling amplitude modulation by RDSOC gives access to the full variety of TFIM configurations.

Next, we simulate a realistic implementation of our proposal based on a LC microcavity with a patterning of the distributed Bragg reflector [74] which realizes an in-plane potential. The potential $\hat{U}(\mathbf{r})$ [equivalent for both pseudospins and defined in 2D real space $\mathbf{r} = (x, y)$]

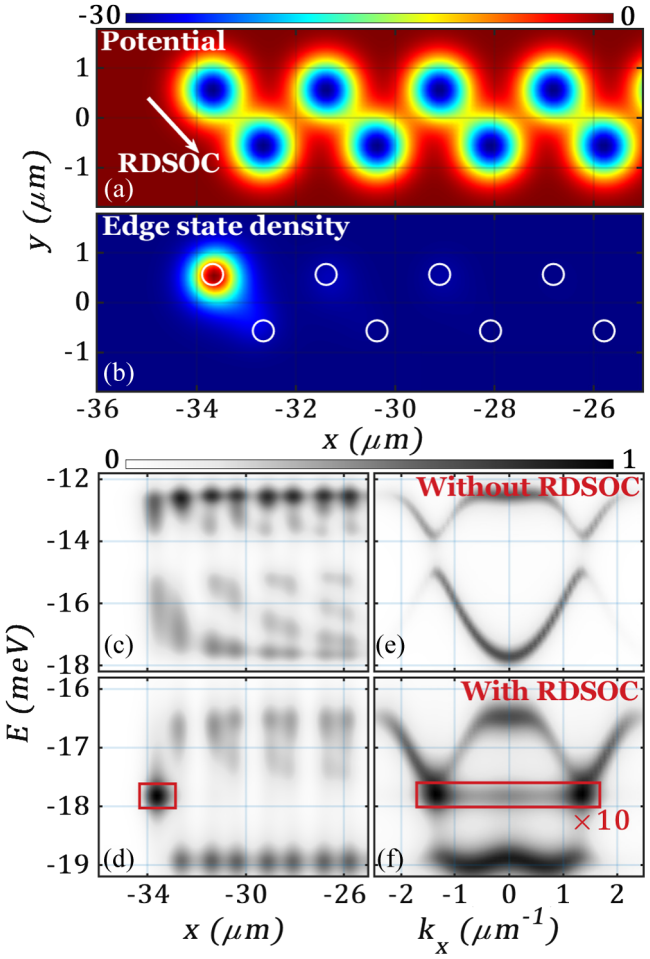

FIG. 3. (a) 2D SSH potential (in meV) constructed out of Gaussian wells with RDSOC aligned along intracell coupling; (b) normalized edge state density; energy spectrum in real (c),(d) and reciprocal (e),(f) spaces in the absence (c),(e) and presence (d),(f) of RDSOC; white-black shows normalized density; the red rectangular shows the edge state [in (f) intensity is increased by 10× for visibility].

corresponding to realistic experimental values is shown in Fig. 3(a) with the RDSOC being oriented along the strong link of the zigzag chain. We perform a simulation beyond the tight-binding approximation by solving the stationary spinor Schrödinger equation with $\hat{H}_{2D} = \hat{H}_0(\mathbf{r}) + \hat{U}(\mathbf{r})$ in 2D (parameters in Ref. [75]), where $\hat{H}_0(\mathbf{r})$ is a Fourier transform of Eq. (1).

Figures 3(c) and 3(e) show the modes in the real and reciprocal spaces without RDSOC. The chain exhibits a clear band gap of 1 meV, but no edge states. Figures 3(d) and 3(f) show the case with nonzero RDSOC ($\alpha = 1.62$ meV μm [67]). A mode strongly localized on the edge [also see Fig. 3(b)] appears within the gap. The asymmetry between the lower and upper bands is enhanced when going beyond the tight-binding model. However, the lowest band is flattened analogously to $\beta = \pi/2$ in the tight-binding model [Figs. 2(b)–2(d)]. These simulations

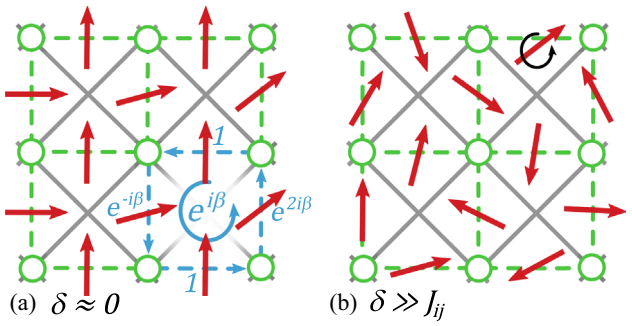

FIG. 4. (a) Harper-Hofstadter and (b) classical XY model realizations based on tunneling (a) phase and (b) amplitude control by RDSOC; green circles and dashed lines represent lattice sites and tunnelings, respectively; gray squares show different electrodes controlling in-plane rotation of RDSOC direction (red arrows) and thus the tunnelings between lattice sites; the blue elements explain the acquisition of phase when encircling a plaquette.

clearly demonstrate the possibility to switch between topologically trivial and nontrivial system states simply by applying voltage. The edge state exhibits period doubling discussed in Ref. [67].

Finally, we consider 2D lattices where the RDSOC orientation is controlled for each individual tunneling. In general, the phases β_{ij} can be controlled by electrodes with patterning, determining the in-plane orientation of RDSOC between every pair of sites (Fig. 4) [76,77]. In the limit of $\delta \approx 0$ [Eq. (3)], the TRS-preserving version of the Harper-Hofstadter model [6,8] is achievable by proper tuning of tunneling phases. As shown in Fig. 4(a), x-dependent rotation of the RDSOC direction for the vertical links gives rise to an increasing phase factor βx that leads to a nonzero round-trip phase $\beta(x+1)-\beta x=\beta$ for each plaquette, independent of its position. The contribution of the horizontal links is zero. The artificial magnetic flux felt by the second spin component is opposite, and the edges of such systems are expected to carry chiral spin currents, as in the quantum spin Hall effect.

In the limit of large detuning $\delta \gg J_{ij}$ [Eq. (4)], the orientation of the RDSOC allows us to control the magnitudes and the signs of the tunneling coefficients [Fig. 4(b)]. With these abritrary tunnelings, the Hamiltonian (4) can be mapped to the classical XY Hamiltonian:

$$\hat{H}_{XY}=\sum_{i\neq j} J\cos\beta_{ij}\cos\left(\eta_i-\eta_j\right), \tag{10}$$

with η_i being the orientation of the in-plane spin i, encoded in the phase of the wave function $\arg\psi_i$ at site i, which allows one to simulate complex spin-liquid phases, superfluids, and superconductors and solve some optimization problems [11,14,78,79]. The dynamical version of the XY model is also known as the Kuramoto network, one of the simplest models describing synchronization and very important in the field of neural networks. Realizations using the suggested LC-based simulator would be compact and benefit from high accessibility to the wave function.

To conclude, we have shown that RDSOC acts as a synthetic gauge field controlling the magnitude and phase of the tunneling coefficients. RDSOC can regulate the topology of a 1D chain and of a 2D lattice (Harper-Hofstadter model). It allows us to simulate spin lattices described by the TFIM and XY Hamiltonians within whole interesting configuration space. We have proposed a realistic implementation using patterned LC microcavities. Interesting perspectives include the non-Hermitian effects [80,81] and photonic nonlinearities [82]. Also, our proposal can be realized in other platforms such as electronic and fermionic atomic systems.

This work was supported by the European Union Horizon 2020 program, through a Future and Emerging Technologies (FET) Open research and innovation action under Grant Agreement No. 964770 (TopoLight). B. P. acknowledges National Science Centre, Poland, Grant No. 2017/27/B/ST3/00271. J. S. acknowledges National Science Centre, Poland, Grant No. 2019/35/B/ST3/04147. D. S. and G. M. acknowledge the support of the projects ANR Labex GaNEXT (ANR-11-LABX-0014), ANR NEWAVE (ANR-21-CE24-0019-01), and of the ANR program "Investissements d'Avenir" through the IDEX-ISITE initiative 16-IDEX-0001 (CAP 20-25).

*Corresponding author.
pavel.kokhanchik@uca.fr

[1] M. Aidelsburger, S. Nascimbene, and N. Goldman, C.R. Phys. **19**, 394 (2018).
[2] T. Ozawa and H. M. Price, Nat. Rev. Phys. **1**, 349 (2019).
[3] I. Bloch, J. Dalibard, and S. Nascimbene, Nat. Phys. **8**, 267 (2012).
[4] P. G. Harper, Proc. Phys. Soc. London Sect. A **68**, 874 (1955).
[5] D. R. Hofstadter, Phys. Rev. B **14**, 2239 (1976).
[6] M. Hafezi, E. A. Demler, M. D. Lukin, and J. M. Taylor, Nat. Phys. **7**, 907 (2011).
[7] M. Hafezi, S. Mittal, J. Fan, A. Migdall, and J. Taylor, Nat. Photonics **7**, 1001 (2013).
[8] M. Aidelsburger, M. Atala, M. Lohse, J. T. Barreiro, B. Paredes, and I. Bloch, Phys. Rev. Lett. **111**, 185301 (2013).
[9] F. D. M. Haldane, Phys. Rev. Lett. **61**, 2015 (1988).
[10] L. Onsager, Phys. Rev. **65**, 117 (1944).
[11] N. G. Berloff, M. Silva, K. Kalinin, A. Askitopoulos, J. D. Töpfer, P. Cilibrizzi, W. Langbein, and P. G. Lagoudakis, Nat. Mater. **16**, 1120 (2017).
[12] M. Nixon, E. Ronen, A. A. Friesem, and N. Davidson, Phys. Rev. Lett. **110**, 184102 (2013).
[13] A. Lucas, Front. Phys. **2**, 5 (2014).
[14] I. M. Georgescu, S. Ashhab, and F. Nori, Rev. Mod. Phys. **86**, 153 (2014).

[15] K. Y. Bliokh and Y. P. Bliokh, Phys. Rev. E **70**, 026605 (2004).
[16] M. Onoda, S. Murakami, and N. Nagaosa, Phys. Rev. Lett. **93**, 083901 (2004).
[17] A. Kavokin, G. Malpuech, and M. Glazov, Phys. Rev. Lett. **95**, 136601 (2005).
[18] C. Leyder, M. Romanelli, J. P. Karr, E. Giacobino, T. C. Liew, M. M. Glazov, A. V. Kavokin, G. Malpuech, and A. Bramati, Nat. Phys. **3**, 628 (2007).
[19] O. Hosten and P. Kwiat, Science **319**, 787 (2008).
[20] K. Y. Bliokh, A. Niv, V. Kleiner, and E. Hasman, Nat. Photonics **2**, 748 (2008).
[21] K. Y. Bliokh, F. J. Rodríguez-Fortuño, F. Nori, and A. V. Zayats, Nat. Photonics **9**, 796 (2015).
[22] Z. Zhang, S. Liang, F. Li, S. Ning, Y. Li, G. Malpuech, Y. Zhang, M. Xiao, and D. Solnyshkov, Optica **7**, 455 (2020).
[23] A. V. Kavokin, J. J. Baumberg, G. Malpuech, and F. P. Laussy, *Microcavities* (Oxford University Press, New York, 2017), Vol. 21.
[24] I. A. Shelykh, G. Pavlovic, D. D. Solnyshkov, and G. Malpuech, Phys. Rev. Lett. **102**, 046407 (2009).
[25] C.-E. Bardyn, T. Karzig, G. Refael, and T. C. H. Liew, Phys. Rev. B **91**, 161413(R) (2015).
[26] M. G. Silveirinha, Phys. Rev. B **92**, 125153 (2015).
[27] D. Solnyshkov and G. Malpuech, C.R. Phys. **17**, 920 (2016).
[28] A. Gianfrate, O. Bleu, L. Dominici, V. Ardizzone, M. De Giorgi, D. Ballarini, G. Lerario, K. West, L. Pfeiffer, D. Solnyshkov *et al.*, Nature (London) **578**, 381 (2020).
[29] F. D. M. Haldane and S. Raghu, Phys. Rev. Lett. **100**, 013904 (2008).
[30] Z. Wang, Y. D. Chong, J. D. Joannopoulos, and M. Soljačić, Phys. Rev. Lett. **100**, 013905 (2008).
[31] Z. Wang, Y. Chong, J. D. Joannopoulos, and M. Soljačić, Nature (London) **461**, 772 (2009).
[32] L. Lu, J. D. Joannopoulos, and M. Soljačić, Nat. Photonics **8**, 821 (2014).
[33] A. V. Nalitov, D. D. Solnyshkov, and G. Malpuech, Phys. Rev. Lett. **114**, 116401 (2015).
[34] T. Karzig, C.-E. Bardyn, N. H. Lindner, and G. Refael, Phys. Rev. X **5**, 031001 (2015).
[35] S. Klembt, T. Harder, O. Egorov, K. Winkler, R. Ge, M. Bandres, M. Emmerling, L. Worschech, T. Liew, M. Segev *et al.*, Nature (London) **562**, 552 (2018).
[36] A. B. Khanikaev, S. Hossein Mousavi, W.-K. Tse, M. Kargarian, A. H. MacDonald, and G. Shvets, Nat. Mater. **12**, 233 (2013).
[37] X. Cheng, C. Jouvaud, X. Ni, S. H. Mousavi, A. Z. Genack, and A. B. Khanikaev, Nat. Mater. **15**, 542 (2016).
[38] L.-H. Wu and X. Hu, Phys. Rev. Lett. **114**, 223901 (2015).
[39] T. Ma, A. B. Khanikaev, S. H. Mousavi, and G. Shvets, Phys. Rev. Lett. **114**, 127401 (2015).
[40] S. Barik, H. Miyake, W. DeGottardi, E. Waks, and M. Hafezi, New J. Phys. **18**, 113013 (2016).
[41] W. P. Su, J. R. Schrieffer, and A. J. Heeger, Phys. Rev. Lett. **42**, 1698 (1979).
[42] J. K. Asbóth, L. Oroszlány, and A. Pályi, Lect. Notes Phys. **919**, 166 (2016).
[43] D. D. Solnyshkov, A. V. Nalitov, and G. Malpuech, Phys. Rev. Lett. **116**, 046402 (2016).
[44] P. St-Jean, V. Goblot, E. Galopin, A. Lemaître, T. Ozawa, L. Le Gratiet, I. Sagnes, J. Bloch, and A. Amo, Nat. Photonics **11**, 651 (2017).
[45] T. H. Harder, M. Sun, O. A. Egorov, I. Vakulchyk, J. Beierlein, P. Gagel, M. Emmerling, C. Schneider, U. Peschel, I. G. Savenko *et al.*, ACS Photonics **8**, 1377 (2021).
[46] Y. A. Bychkov and É. I. Rashba, JETP Lett. **39**, 66 (1984), http://jetpletters.ru/ps/1264/article_19121.shtml.
[47] G. Dresselhaus, Phys. Rev. **100**, 580 (1955).
[48] B. A. Bernevig, J. Orenstein, and S.-C. Zhang, Phys. Rev. Lett. **97**, 236601 (2006).
[49] J. D. Koralek, C. P. Weber, J. Orenstein, B. A. Bernevig, S.-C. Zhang, S. Mack, and D. Awschalom, Nature (London) **458**, 610 (2009).
[50] Y.-J. Lin, K. Jiménez-García, and I. B. Spielman, Nature (London) **471**, 83 (2011).
[51] N. Dahan, Y. Gorodetski, K. Frischwasser, V. Kleiner, and E. Hasman, Phys. Rev. Lett. **105**, 136402 (2010).
[52] K. Frischwasser, I. Yulevich, V. Kleiner, and E. Hasman, Opt. Express **19**, 23475 (2011).
[53] N. Shitrit, I. Yulevich, V. Kleiner, and E. Hasman, Appl. Phys. Lett. **103**, 211114 (2013).
[54] N. Shitrit, I. Yulevich, E. Maguid, D. Ozeri, D. Veksler, V. Kleiner, and E. Hasman, Science **340**, 724 (2013).
[55] V. Yannopapas, Phys. Rev. B **83**, 113101 (2011).
[56] Y. Plotnik, M. A. Bandres, S. Stützer, Y. Lumer, M. C. Rechtsman, A. Szameit, and M. Segev, Phys. Rev. B **94**, 020301(R) (2016).
[57] I. A. Shelykh, A. V. Nalitov, and I. V. Iorsh, Phys. Rev. B **98**, 155428 (2018).
[58] K. Rechcińska, M. Król, R. Mazur, P. Morawiak, R. Mirek, K. Łempicka, W. Bardyszewski, M. Matuszewski, P. Kula, W. Piecek *et al.*, Science **366**, 727 (2019).
[59] J. Ren, Q. Liao, F. Li, Y. Li, O. Bleu, G. Malpuech, J. Yao, H. Fu, and D. Solnyshkov, Nat. Commun. **12**, 689 (2021).
[60] L. Polimeno, G. Lerario, M. De Giorgi, L. De Marco, L. Dominici, F. Todisco, A. Coriolano, V. Ardizzone, M. Pugliese, C. T. Prontera *et al.*, Nat. Nanotechnol. **16**, 1349 (2021).
[61] Z. Yan and S. Wan, Europhys. Lett. **107**, 47007 (2014).
[62] M. Bahari and M. V. Hosseini, Phys. Rev. B **94**, 125119 (2016).
[63] Y. Yao, M. Sato, T. Nakamura, N. Furukawa, and M. Oshikawa, Phys. Rev. B **96**, 205424 (2017).
[64] Z.-H. Liu, O. Entin-Wohlman, A. Aharony, J. Q. You, and H. Q. Xu, Phys. Rev. B **104**, 085302 (2021).
[65] Z.-H. Liu and H. Xu, J. Appl. Phys. **130**, 174301 (2021).
[66] Y. Aharonov and A. Casher, Phys. Rev. Lett. **53**, 319 (1984).
[67] See Supplemental Material at http://link.aps.org/supplemental/10.1103/PhysRevLett.129.246801 for the discussion of uniform RDSOC in a monomer chain, Hamiltonian of the SSH lattice with modulated RDSOC in linear polarization basis, period-doubling in the tight-binding model and in the solution of the Schrödinger equation, topology of the SSH chain depending on RDSOC orientation, dependence of detuning δ on voltage V, RDSOC magnitude, and control of RDSOC direction.
[68] J. Zak, Phys. Rev. Lett. **62**, 2747 (1989).
[69] P. De Gennes, Solid State Commun. **1**, 132 (1963).
[70] P. Pfeuty, Ann. Phys. (N.Y.) **57**, 79 (1970).

[71] T. Kadowaki and H. Nishimori, Phys. Rev. E **58**, 5355 (1998).
[72] P. Calabrese, F. H. L. Essler, and M. Fagotti, Phys. Rev. Lett. **106**, 227203 (2011).
[73] M. Heyl, A. Polkovnikov, and S. Kehrein, Phys. Rev. Lett. **110**, 135704 (2013).
[74] F. Scafirimuto, D. Urbonas, M. A. Becker, U. Scherf, R. F. Mahrt, and T. Stöferle, Commun. Phys. **4**, 39 (2021).
[75] SSH-like zigzag potential $U(x, y)$ is constructed out of Gaussian potential wells with 30 meV depth, 1 μm FWHM, and 1.53 (1.7) μm intracell (intercell) distance, respectively. The cavity photon mass is $m = 1.6 \times 10^{-5} m_e$, where m_e is an electron mass; we take value of $\delta = 5.5$ meV and introduce Lorentzian broadening with 0.5 meV FWHM.
[76] A. Mochizuki, Crystals **11**, 337 (2021).
[77] A. Mochizuki, J. Mol. Liq. **267**, 456 (2018).
[78] M. Parto, W. Hayenga, A. Marandi, D. N. Christodoulides, and M. Khajavikhan, Nat. Mater. **19**, 725 (2020).
[79] R. Tao, K. Peng, L. Haeberlé, Q. Li, D. Jin, G. R. Fleming, S. Kéna-Cohen, X. Zhang, and W. Bao, Nat. Mater. **21**, 761 (2022).
[80] R. Su, E. Estrecho, D. Bieganska, Y. Huang, M. Wurdack, M. Pieczarka, A. G. Truscott, T. C. H. Liew, E. A. Ostrovskaya, and Q. Xiong, Sci. Adv. **7**, eabj8905 (2021).
[81] M. Król, I. Septembre, P. Oliwa, M. Kędziora, K. Łempicka-Mirek, M. Muszyński, R. Mazur, P. Morawiak, W. Piecek, P. Kula *et al.*, Nat. Commun. **13**, 5340 (2022).
[82] N. Pernet, P. St-Jean, D. D. Solnyshkov, G. Malpuech, N. Carlon Zambon, Q. Fontaine, B. Real, O. Jamadi, A. Lemaitre, M. Morassi *et al.*, Nat. Phys. **18**, 678 (2022).